THE JOURNAL OF PHYSICAL CHEMISTRY C
A JOURNAL OF THE AMERICAN CHEMICAL SOCIETY

pubs.acs.org/JPCC
Article

Surface, Interface, Compression and Formation Energies of Bimetallic Ag/Pt(111) and Ag/Pd(111) Surfaces from First-Principles

Published as part of The Journal of Physical Chemistry C virtual special issue "Francesc Illas and Gianfranco Pacchioni Festschrift".

Sung Sakong, Axel Groß, and R. Jürgen Behm*

Cite This: J. Phys. Chem. C 2024, 128, 13558–13567

ABSTRACT: As an example for bimetallic surfaces in general, we have systematically investigated the thermodynamic surface properties of bimetallic Ag/Pt(111) and Ag/Pd(111) surfaces, including pseudomorphic Ag film covered surfaces and $M_1Ag_3/M(111)$ (M = Pt, Pd) monolayer surface alloys, by periodic density functional theory calculations. Employing larger, symmetric unit cells and slabs, we could determine the surface energy of the asymmetric surface region without interference with contributions from the bottom side of the slab used in these calculations. In the calculation of formation energies, we distinguish between bulk and slab formation energies. Interface energies are derived from appropriately structured bulk unit cells, and corrected for contributions arising from the compression of pseudomorphic film layers (compression energy). While the general trends for the Pt(111)- and Pd(111)-based systems are rather similar, we also find specific differences. Possible reasons for these trends and the specific discrepancies will be addressed. We propose that the procedures presented here are of general validity and can be applied also to other complex surfaces.

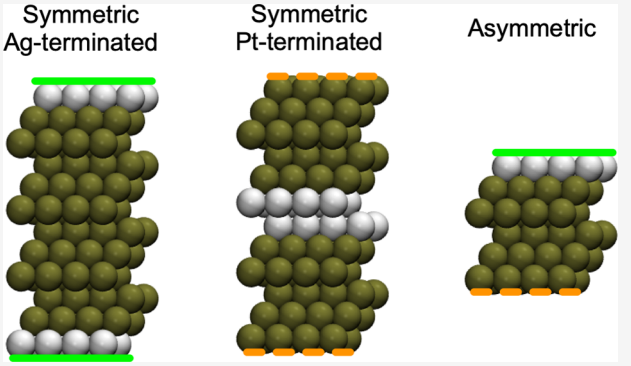

1. INTRODUCTION

The structure, chemical composition as well as physical and chemical properties of multicomponent solid surfaces are often dominated by their (specific) surface energy and their formation energy. For instance, the wetting properties of surfaces or the thermodynamic growth modes of thin films[1,2] are determined by the surface and interface energies of a supporting solid (substrate) and a thin film deposited thereon (deposit), where the specific surface energy is defined by the energy required to create additional surface area (see also Section 3.1). Unfortunately, the quantitative determination of these parameters is experimentally challenging, and also theoretically, there are problems, at least for a first-principles atomic scale determination. Using periodic density functional theory (DFT) based calculations, surface energies of solids have been commonly determined by cleaving a bulk crystal, which can be calculated by subtracting the energy of the bulk solid (no surface contribution) from the energy of a slab with a defined surface area.[3] Here, the bulk is infinitely extended by repeating a unit cell periodically in all three dimensions, while the slab includes a vacuum layer between slabs containing bulk motives, which breaks the crystal symmetry in one direction. The slab is periodic only in two dimensions and includes surface effects. This approach requires that the two new surfaces are identical also in detail, which for single-component surfaces is not problematic. In most DFT calculations, slabs are modeled by a few atomic layers and relaxed only in the topmost layers, while in the bottom layers, the atoms are frozen at their bulk positions. In that case, the calculated surface energy is an average from the relaxed and unrelaxed slab surfaces. The averaged value is still close to the surface energy for a monatomic slab, but with a small energy gain by the surface relaxation. To correct for this, the slab needs to be sufficiently thick that both new surfaces can be relaxed and nevertheless contain a bulk-like part in the center.

More complex is the situation in the case of bimetallic surfaces, including metal film covered surfaces or surface alloys, or generally for multicomponent surfaces.[4,5] Staying at the case of bimetallic surfaces, or specifically, a metal substrate surface covered by an ultrathin film of another metal, the calculated energy difference between the slab and the bulk energies of the

Received: April 22, 2024
Revised: July 25, 2024
Accepted: July 26, 2024
Published: August 7, 2024

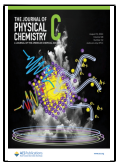

two components now includes not only averaging between the different surfaces on both sides of the slab, but also the energy required or released upon formation of the internal interface between the two metals. For a more detailed understanding and a precise determination of the various energy contributions, these have to be determined separately. Comparable problems also exist for the determination of the formation enthalpy. Furthermore, in a more detailed picture, the neighborhood of the new surface before the cleavage, on the other side of the cleavage plane, is not well-defined, which will affect the cleavage energy.

This is the topic of the present publication, where, as part of an extensive series of combined experimental and theoretical studies on the structure, stability, electronic properties and adsorption behavior of structurally well-defined bimetallic PdAg/Pd(111)[6−11] and PtAg/Pt(111)[12−16] surfaces, we report results of a theoretical study of the first-principles determination of the surface energy and formation energy of different Ag/Pt(111) and PtAg/Pt(111) surfaces. In addition, for a better understanding of the underlying electronic effects, we will compare the resulting trends with those obtained for similar Ag/Pd(111) and PdAg/Pd(111) surfaces. Pt and Pd are well-known for their close similarity in their structural, electronic, and chemical properties, e.g., in lattice constant or number of d-electrons.[17] Nevertheless, there are distinct differences in their surface properties, e.g., in alloy formation, with a tendency for two-dimensional (2D) phase separation in PtAg/Pt(111) while this is absent in PdAg/Pd(111),[8,13,16,18] in the adsorption behavior, with a pronounced site preference in CO adsorption on Pd(111) in contrast to small differences in Pt(111),[13,19] or in surface diffusion of H_{ad} or CO_{ad}.[20−26]

In the following, after a brief description of the computational model, we will first describe and discuss our approach for determining the surface energies and formation enthalpies. We will then present results for the different Pt(111)- and Pd(111)-based bimetallic systems, discuss trends and specific differences between Pt(111)- and Pd(111)-based systems, and discuss possible reasons for specific discrepancies. Finally, we will briefly comment on the general validity and applicability of the approach presented here and on possible limitations.

2. COMPUTATIONAL DETAILS

The total energies of the bulk and slab alloys were obtained by performing density functional theory calculations with the plane wave-based Vienna ab initio simulation package (VASP) code (version 6.4.2).[27] We employed the Perdew−Burke−Ernzerhof (PBE)[28] functionals and the projector augmented wave (PAW) potentials[29] to describe exchange-correlation interactions and the ionic cores, respectively.[30,31] The electronic wave functions of the quasiparticles were expanded using a plane-wave basis set up to a cutoff energy of 300 eV, which is larger than the default values preset in the potentials for platinum, palladium, and silver. Dipole moment corrections were not necessary for the symmetric slabs because of the cancelation by the identical surfaces oriented in opposite directions. For the asymmetric slabs they were disregarded because of the large size of the vacuum region.

The bulk lattice parameters (d_b) of Pt, Pd, and Ag were computed using an (1 × 1 × 1) *fcc* unit cell with a 24 × 24 × 24 *k*-point grid. The resulting bulk lattice parameters of Pt, Pd, and Ag are 3.96, 3.93, and 4.14 Å, respectively. The lattice parameters from the PBE calculations exceed the experimental values of 3.92, 3.89, and 4.09 Å by about 1%.[32]

Symmetric mono- and bimetallic bulk systems were described by 12 atom layers in (111) orientation with a (2 × 2) lateral unit cell, i.e., the bulk unit cell consists of 48 atoms. As will be described in more detail in Section 3.1, this included two 6-layer subsystems with a Pt(111) or Pd(111) substrate and Ag containing layers in the top, which were arranged in a mirrored configuration. In each subsystem, two layers of the host elements (Pt or Pd) were fixed at their bulk positions. The guest element Ag atoms replaced the host atoms in the middle of the relaxed layers, forming a mirrored layer configuration along the *c*-direction. The configurations of the remaining eight layers were optimized together with the unit cell size in the *c*-direction. The compressed Ag layers with the lateral lattice constants of Pt and Pd were computed using 12 fully relaxed Ag layers with adjustable *c*-axis size.

The bimetallic slab configurations, which equally contained 12 layers, were created by inserting a vacuum layer larger than 12 Å between the symmetric slabs. The four middle layers of the host elements were fixed at their bulk positions, while the four upper and bottom layers were fully relaxed. Asymmetric bimetallic slabs comprised six atom layers, i.e., 24 atoms, which were separated by a vacuum layer of 24 Å. The two bottom layers of the host elements were fixed at their bulk positions, while the upper four layers were fully relaxed. The first Brillouin zone of the bimetallic slabs was integrated using a 6 × 6 × 1 *k*-point grid. The fully relaxed configurations were determined by the electronic energy convergence and the forces on ions with criteria of 1×10^{-6} eV and 0.01 eV/Å, respectively. Finally, we would like to add that due to error cancellation in these very similar calculations we expect relative energy changes by 0.01 eV to be significant.

3. RESULTS AND DISCUSSION

3.1. Determination of Surface Energies and Formation Enthalpies of Bimetallic Surfaces. The surface energy or, more correctly, the specific surface energy of a solid E_S is classically defined as the energy E required to reversibly increase the surface area A of a given solid, while keeping the mass constant

$$E_S = \frac{\delta E}{\delta A} \tag{1}$$

For simplicity, we will in the following use the term "surface energy" for E_S. Changing to a computational approach, and starting with a homogeneous single component system, the surface energy can be determined as the crystal cleavage energy according to eqs 2a or 2b

$$E_S = \frac{1}{2A}(E_{slab} - E_{bulk}) \tag{2a}$$

$$E_S = \frac{1}{2A}(E_{slab} - n \cdot E_b) \tag{2b}$$

where the slab consists of a few layers of the respective material (Figure 1a). A denotes the slab surface area, and E_{slab} is the total energy of the slab. In eq 1a, E_{bulk} is the total energy of the corresponding bulk unit cell. Alternatively, one can also use eq 2b, where the bulk energy is given by the number (n) and the (atomic) bulk energy E_b of the respective atoms. These equations assume that the two sides of the slab have similar surface energies. However, as mentioned before, this neglects the fact that in computational approaches the atoms on the bottom surface are commonly not relaxed. In the case of

https://doi.org/10.1021/acs.jpcc.4c02619
J. Phys. Chem. C 2024, 128, 13558−13567

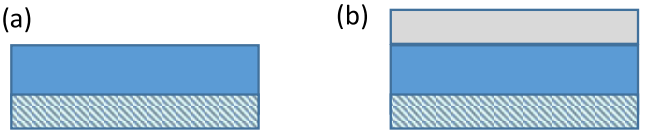

Figure 1. Slab models for monometallic (a) and bimetallic (b) unit cells and slabs, illustrating their asymmetric nature (blue dashed: frozen substrate bottom layers, blue: relaxed substrate layers at/close to the surface, gray: deposit).

bimetallic surfaces (Figure 1b), this furthermore neglects that the two surfaces differ in their chemical composition. In these cases, one obtains an average value of the surface energy of the two surfaces, with unknown contributions of the upper and lower surface. Depending on the nature of the upper and lower surfaces, the differences can be significant. Furthermore, we have to define the structure and composition of the bulk unit cell on the other side of the cleavage plane.

To resolve these problems, we designed a modified system consisting of two of the original asymmetric slabs. These are arranged in a mirrored configuration, such that the resulting new slab is symmetric with respect to the sequence of layers, as illustrated in Figure 2. Here Ag1L, Ag2L and Ag3L denote systems where the Pt substrate is covered by 1 layer (Ag1L), 2 layer (Ag2L), or 3 layer (Ag3L) pseudomorphic Ag films. We also consider surface alloys with a Pt_1Ag_3 topmost layer supported on 5 layers of Pt(111), which resemble the Ag1L system, but with a mixed topmost layer. The two superscripts a and b ($Pt_1Ag_3^{(a)}$ and $Pt_1Ag_3^{(b)}$) refer to systems with different stacking of the mixed layers at the cleavage plane, where in one case a Pt atom at the cleavage plane is located on a Pt_1Ag_2 hollow site and in the other case on a Ag_3 site. Structurally, the whole bulk maintains its fcc stacking. Different from previous calculations,[10,11,19] the original slab comprises 6 layers rather than 5 layers, with two unrelaxed layers and 4 fully relaxed layers, to allow for a continuous ABCABC··· type stacking. Combining two of the 6-layer slabs in a mirrored configuration results in a 12-layer symmetric slab/supercell, with either two film surfaces at the outside of the slab/supercell (here: Ag-terminated), or two substrate surfaces (here: Pt-terminated). While on a first view these systems in Figure 2 may be considered as superlattices, there is an important difference: In superlattices with about equally thick pseudomorphic multilayers of materials A and B one would expect the lateral lattice constants to be somewhere in between those of the two materials upon relaxation. In contrast, in the systems presented in Figure 2, we intentionally fixed the lateral lattice constant to that of Pt(111), as the frozen bottom layers were intended to be representative of a Pt bulk.

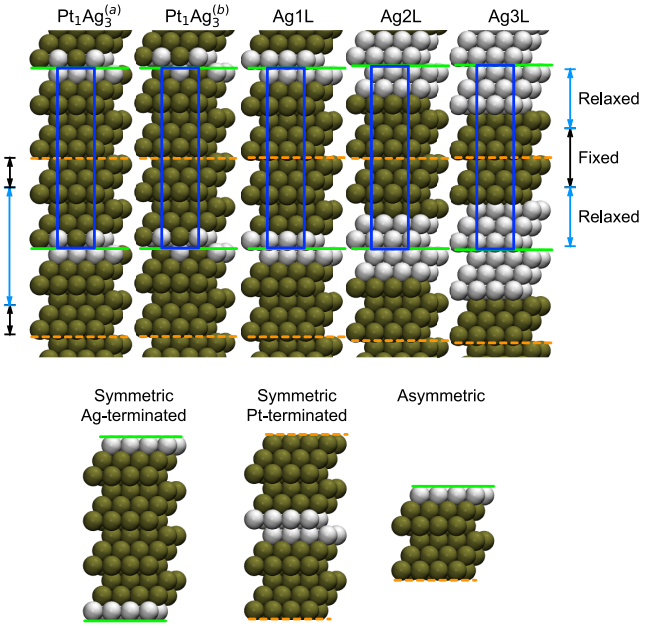

Figure 2. Models of the symmetric 12-layer bulk supercells (top row) and of the similar size Ag-terminated and Pt-terminated symmetric slabs (here: for Ag1L, bottom row) used in this work for calculation of the surface energies, compression energies, interface energies and formation energies of the different Ag/Pt(111) and Ag/Pd(111) systems (light gray: Ag, olive: Pt or Pd). The blue box shows the unit cell of the bulk. Cleaving along the planes indicated by the green solid and orange dashed lines in the bulk presentations generates the symmetric Ag terminated slab and the symmetric Pt-terminated slab, respectively, from the periodic bulk. In addition, we also show the asymmetric 6-layer slab (bottom row), which is normally used for such calculations (here: for the Ag1L system).

Using a similar type 12-layered bulk supercell as a reference, the surface energy of either of the surfaces can be determined separately as

$$E_{S,dep} = \frac{1}{2A}(E_{slab,dep} - E_{bulk}) \quad (3)$$

or

$$E_{S,sub} = \frac{1}{2A}(E_{slab,sub} - E_{bulk}) \quad (4)$$

where the subscripts dep and sub denote slabs/bulk unit cells that are terminated by deposit or substrate surface layers, respectively. It is important to note that in this model the bulk reference is constructed in such a way that the neighborhood of the cleavage plane is symmetric with respect to the sequence of layers. In this case, the substrate or bulk terminated slabs can be constructed from the periodic bulk by positioning the cleavage planes, as indicated for the deposit terminated (Ag-terminated) and the bulk terminated (Pt-terminated) slabs by the green solid lines and the orange dashed lines in Figure 2.

Alternatively, these surface energies can also be determined by cleaving the symmetric 12-layer slab ($E_{slab,12L}$) into two 6-layer slabs ($E_{slab,6L}$). Depending on the choice of the 12-layer slab, this yields either the surface energy of the relaxed deposit surface (symmetric Pt-terminated 12-layer slab) or the unrelaxed substrate surface (symmetric Ag-terminated 12-layer slab).

$$E_S = \frac{1}{2A}(E_{slab,12L} - 2E_{slab,6L}) \quad (5)$$

Since the slabs terminated by the deposit or the substrate layers refer to the same bulk structure, the bulk energy (E_{bulk}) has to be identical.

For complex systems such as bimetallic systems, both the bulk unit cell and the slab may contain interfaces between substrate and deposit, which lead to interactions between substrate and deposit atoms in a mixed system, exceeding the mean interactions calculated from the atomic bulk energies. For a system with 2 phases or 2 components, the interface energy E_{int} can be defined as the additional energy of the system due to the presence of the interface, in addition to the difference of the surface energies.[1,2] Similar to the surface

https://doi.org/10.1021/acs.jpcc.4c02619
J. Phys. Chem. C 2024, 128, 13558−13567

energy, this is also normalized to the surface area of the interface A. Furthermore, these systems may contain contributions due to lateral compression of layers, e.g., in the case of pseudomorphic deposit film on a substrate. In that case, the sum of the related interface and compression energies E_{int} and E_{comp} is given by the difference between the energy of the bulk unit cell and the sum of the bulk energies of the respective metals, $E_{b,i}$, according to

$$E_{int} + E_{comp} = \frac{1}{2A}\left(E_{bulk} - \sum_i n_i \cdot E_{b,i}\right) \quad (6)$$

Here, E_{int} and E_{comp} represent the interface and compression energies per Å^2, respectively, and E_{bulk} again denotes the energy of the bulk unit cell, which in this case may consist of several atoms of different nature. i refers to the different species in the system, and n_i and $E_{b,i}$ indicate the number and (atomic) bulk energies of these species, respectively. Note that we have to divide by 2A since the unit cell contains two identical interfaces. The compression energy E_{comp} of a guest (deposit) metal can be derived from the energy difference between a bulk unit cell of the laterally compressed guest metal with the lattice constant of the host (substrate) metal $E_{bulk,comp}$ and a bulk unit cell of the guest metal in its natural lattice. For direct comparison with E_{int} we again normalize the energy with respect to the surface area of the unit cell by dividing it by the surface area 2A.

$$E_{comp} = \frac{1}{2A}(E_{bulk,comp} - E_{bulk}) \quad (7)$$

Note that in this case all energies will vary with the number of compressed layers, which is not the case when normalizing it to the number of guest atoms n_{dep} in the unit cell.

$$E^0_{comp} = \frac{1}{n_{dep}}(E_{bulk,comp} - E_{bulk}) \quad (8)$$

Thus, it is highly important to maintain a consistent normalization of the energy values.

For the formation energy E_f, we distinguish whether this refers to the bulk ($E_{f,bulk}$) or the slab ($E_{f,slab}$) formation. The bulk formation energy is defined as the difference between the energy of the bulk unit cell and the sum of the bulk atomic energies $E_{b,i}$, according to

$$E_{f,bulk} = \frac{1}{2A}\left(E_{bulk} - \sum_i n_i \cdot E_{b,i}\right) \quad (9)$$

Comparison of eqs 6 and 9 shows that this is identical with the sum of the interface energy and the compression energy, $E_{int} + E_{comp}$. Here it should be noted that the bulk formation energy is often normalized to the number of atoms or surface atoms in the bulk unit cell rather than to the surface area 2A.

Because of the symmetric nature of the unit cell, with "surfaces" on the top and on the bottom side of the 12-layer cell/slab, the bulk formation energy is normalized by 2A rather than by A. The resulting energies given later in this paper are therefore characteristic for a 6-layer slab with 24 atoms.

The slab formation energy $E_{f,slab}$, which describes the change in slab energy from the initial single-component slab ($E_{slab,ini}$) upon exchange of n_i atoms of species i to/from a reservoir of that respective species to the final bi- or multicomponent slab, is derived from the energy difference of the final slab ($E_{slab,fin}$) on the one hand and of the initial slab ($E_{slab,in}$), the numbers n_i and the bulk energies E_i of the exchanged species atoms on the other hand[33]

$$E_{f,slab} = \frac{1}{2A}\left(E_{slab,fin} - E_{slab,in} - \sum_i n_i \cdot E_{b,i}\right) \quad (10)$$

where the sum runs over the different species i to be exchanged. This definition also indicates that for physical reasons the calculation of a slab formation energy makes sense only for bi- or multicomponent slabs. where only part of the atoms in the initial slab was exchanged, while for single component systems, i.e., for complete exchange of the atoms in the initial slab, the use of this reference system would be arbitrary.

Combining eqs 6 and 9 for the bulk formation energies $E_{f,bulk}$ or eqs 3, 6, and 10, respectively, for the slab formation energies $E_{f,slab}$, the two formation energies can be represented as a function of the surface energies, interface energies and compression energies.

$$E_{f,bulk} = E_{int} + E_{comp} \quad (11)$$

$$E_{f,slab} = \Delta E_S + E_{int} + E_{comp} \quad (12)$$

where ΔE_S denotes the difference in surface energies of the final slab ($E_{S,fin}$) and of the initial slab ($E_{S,in}$), respectively (see also Section S1 in the Supporting Information (SI)). Hence, the two formation energies differ in such a way that in the second case also changes in the surface energies will be included in the formation energies, which may be much larger than, e.g., contributions from interface or compression energies in the bulk. This will be illustrated in more detail in the next section. Here it should also be noted that all energy changes occurring upon cleaving the bulk crystal are attributed to the surface energy, meaning that the interface energy and the compression energy in the bulk and in the slab are assumed to be identical. Possible changes in these numbers upon cleaving the bulk crystal, which may occur in particular if the interface is close to the surface, would appear in the calculated value of the corresponding surface energy. From the changes in interlayer spacing between Pt and Ag layer in the Ag1L, Ag 2L and Ag3L systems upon cleavage, which are 0.003, 0.009, and 0.000 Å, respectively, we estimate an upper limit of such cleavage induced changes in interface energy of 1 meV Å^{-2} at most. Similarly, based on the marginal differences (mostly <0.01 Å) in the interlayer spacings between layers 4 and 5 (both Pt, relaxed interlayer spacing) and between layers 5 and 6 (both Pt, fixed bulk-like interlayer spacing), effects resulting from the bulk-like, unrelaxed interlayer spacing between the two Pt bottom layers can be disregarded in this discussion.

Here we would also like to address conceptual differences to an earlier theoretical study by Tersoff,[34] where the role of strain effects and lattice mismatch in the formation of surface confined alloy systems, as compared to bulk intermixing, was investigated. The main difference between the approach by Tersoff, which is based on the use of surface energies and interface energies, and our approach is that in the former study strain energies are incorporated in the interface energy, while we try to separate strain effects from effects arising from the chemical interaction between substrate and deposit, representing them as compression energy and interface energy. This separation is done by determining the compression energy from the energy needed to laterally compress a bulk crystal (eq 7). The interface energy is then determined by subtracting the

https://doi.org/10.1021/acs.jpcc.4c02619
J. Phys. Chem. C 2024, 128, 13558−13567

compression energy from the bulk formation energy $E_{f,bulk}$ (eqs 6 and 9). Hence, this separation is possible only with the assumption that the compression energy does not differ in the bulk and at the surface. Since the total energy difference between two systems with a Ag layer at the surface or below would be determined correctly in our calculations, deviations arising from the assumption of a layer-independent compression energy would appear as similar changes in the interface energy.

In total, in Section 3.1, we present the general ideas and concepts used to determine surface energies, interface energies, compression energies and formation energies in complex bimetallic systems.

3.2. Surface Energies of Different Bimetallic Ag/Pt(111) Systems. *3.2.1. Ag-Terminated Ag/Pt(111) Systems.* Next, we apply these different energy relations to a number of Ag/Pt(111) based model systems, including Pt(111) substrates covered by $n = 1-3$ pseudomorphic layers of Ag, as well as a Pt(111) substrate covered by a monolayer Pt_1Ag_3 surface alloy. We are well aware of the fact that experimentally only Ag monolayer films were found to grow pseudomorphically, while for bilayer and thicker films the formation of a unidirectionally expanded (striped) phase or, upon annealing, a trigonal incommensurate phase occurs, where strain is relieved isotropically.[35,36] Nevertheless, the data derived here provide detailed insight in stability trends. Furthermore, they illustrate also the advantage of theory that it can give access to systems which are conceptually simple and can serve as model systems, but can hardly be realized experimentally.

Using the symmetric supercells and slabs indicated in Figure 2, application of eq 3 leads to the surface energies for the Ag-terminated surfaces, which are indicated as blue bars in Figure 3a. In addition, the surface energies are listed in Table S1 in the SI. Interestingly, the surface energy calculated for the laterally compressed Ag is essentially identical to that of the bulk Ag. Here, it is important to note that for the laterally compressed Ag we used the bulk energy of the compressed Ag as a reference in eq 1a and not that of the natural Ag bulk, as in ref 19. Using the natural bulk Ag as a reference would increase the calculated surface energy by half of the compression energy of the 12-layer bulk (see below), i.e., by about 18 meV Å^{-2} (Table S1). The similar magnitude of the surface energies can at least qualitatively be explained by the fact that for the laterally compressed Ag the distances between Ag layers are larger and therefore the surface bonds are weaker than for bulk Ag. On the other hand, due to the larger unit cell of bulk Ag there are fewer Ag−Ag bonds per surface area, which seems to compensate the weaker bonding per Ag surface atom. For the pseudomorphic Ag film covered surfaces, we find a significantly higher surface energy for the monolayer film (Ag1L), while for the bilayer (Ag2L), and trilayer (Ag3L) Ag films the surface energies closely resemble that of the pure Ag surfaces. Based on the principle of constant bond order, one would expect the opposite effect for the Ag1L system. Since the Pt−Ag bonds are stronger than Ag−Ag bonds, one would expect the bonds of the Ag surface layer to another Ag layer, which are broken during crystal cleavage, to be weaker than similar bonds in a pure Ag system. Such discrepancies had been explained by long-range effects, which must be present on top of short-range effects following the bond-order principle.[37] For the surface alloys, we considered two cases, one where the underlying Pt atom is underneath a Pt_1Ag_2 hollow site and one where this is underneath a Ag_3 hollow site. In both cases, the surface energies are considerably higher than obtained for the Ag bulk and Ag multilayer films, but lower than that of the Ag1L system. This can simply be understood as a consequence of the stronger Pt−Ag and Pt−Pt bonds as compared to the Ag−Ag bonds.

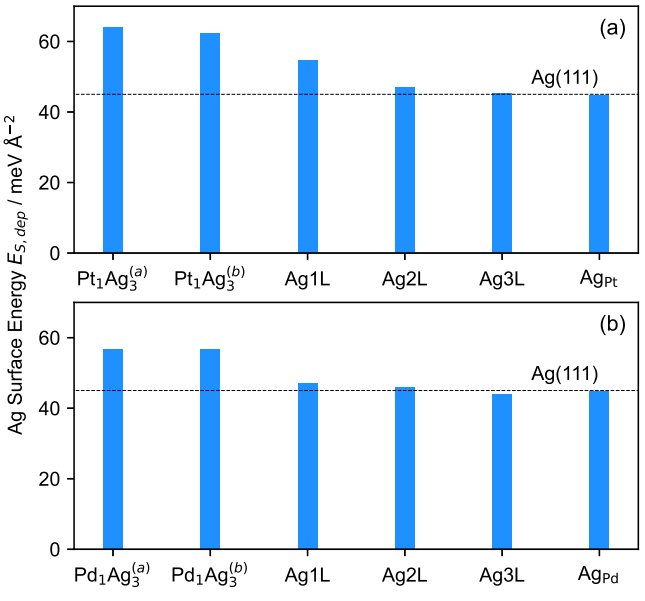

Figure 3. (a) Surface energies E_S of different Ag-terminated bimetallic Ag/Pt(111) systems and of the compressed Ag bulk (details see text). The dashed line indicates the surface energy of Ag(111). (b) Similar plots for the Ag/Pd(111) systems. The exact values are listed in Table S1.

Similar calculations were performed also for Ag/Pd(111) systems. While the general trends are comparable to those in the Ag/Pt(111) system, they differ in the surface energy of the Ag1L system. For the Ag/Pd(111) systems, the surface energy of the Ag1L system resembles more those of the other Ag film terminated surfaces and of the pure Ag surfaces, while for the Ag/Pt(111) systems there is a significant difference. Obviously, for Ag/Pd(111) these long-range effects are much weaker than for the corresponding Ag/Pt(111) system. The two surface alloys are higher in surface energy than the Ag film systems, although the difference is not as pronounced as in the Ag/Pt(111) systems. This difference can be understood from the weaker Ag−Pd interactions that have to be broken during cleavage as compared to the Ag−Pt interactions.

3.2.2. Pt-Terminated Ag/Pt(111) Systems. Similar calculations were performed for the Pt-terminated 12-layer slab (eq 4). In this case, one would expect only small deviations from the Pt(111) surface energies, since the atomic positions of the Pt surface layers were frozen on the bulk positions and deviations from the Pt(111) surface energy can only result from electronic effects induced by the relaxed Pt and Ag layers underneath the frozen 2 surface layers.

In general, the calculated surface energies of the Pt-terminated surfaces with their fixed bulk positions are very close to those of the corresponding Pt(111) and Pd(111) surfaces (Figure 4 and Table S1). Differences are only visible on a magnified scale (cyan bars in Figure 4c). Interestingly, these differences closely follow the trend obtained for the Ag-terminated surfaces. There is very little difference between the surface energies of the Pt-terminated surfaces in the Ag2L and Ag3L systems and that of Pt(111), indicating that electronic

https://doi.org/10.1021/acs.jpcc.4c02619
J. Phys. Chem. C 2024, 128, 13558−13567

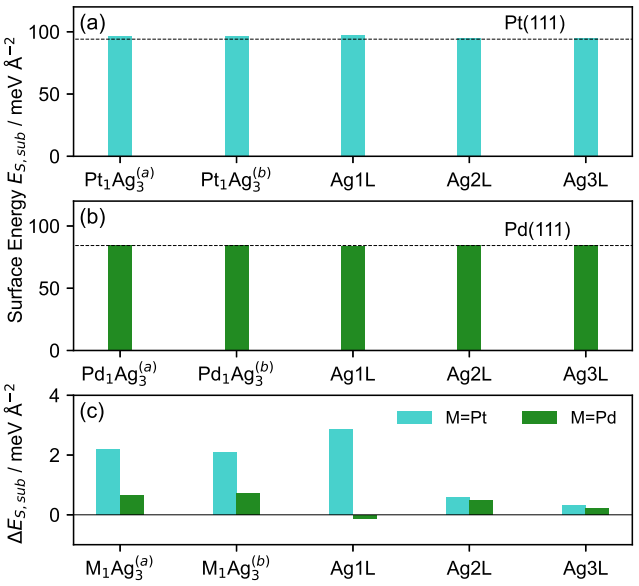

Figure 4. (a) Surface energies of the different Pt-terminated bimetallic Ag/Pt(111) systems (cyan) calculated from the symmetric 12-layer slab and (b) the same for the Pd-terminated bimetallic Ag/Pd(111) systems. The dashed lines indicate the surface energies calculated for the corresponding 12-layer slabs of Pt(111) and Pd(111), respectively. (c) Difference between the surface energies calculated this way and those calculated for similar Pt(111) and Pd(111) slabs, respectively, on a magnified scale. The exact values are listed in Table S1.

modifications of the frozen Pt surface layers induced by the underlying Ag bilayer and trilayer films are very small. This fits nicely to our earlier conclusion that the interface between Pt and the Ag layers is bulk-like for the Ag2L and Ag3L systems, leading to Ag(111)-like surface energies of the Ag-terminated surfaces. In contrast, there is a bigger difference between the surface energy of the Pt-terminated surface and that of Pt(111) for the Ag1L system. This closely resembles our observations for the Ag-terminated surface, and also, in this case, the effect cannot be explained by short-range interactions following the constant bond order principle. The resulting electronic modifications due to the Pt−Ag interface are obviously of long-range nature, since they are felt at the Pt surface layer even over three Pt layers in between. For the mixed layer Pt_1Ag_3 systems, the differences in surface energies are slightly smaller than in the Ag1L film system, in agreement with expectations for a more Pt-like layer.

Finally we note that the differences with respect to the Pt(111) surface energy also demonstrate the magnitude of possible deviations, which would be introduced when calculating the surface energy of the Ag-terminated surface from the mean surface energy of an asymmetric 6 layer slab according to eq (2), i.e., from the difference between the surface energies of that slab and that of Pt(111).

The corresponding calculations of the surface energies of the Pd-terminated surfaces in Ag/Pd(111) systems revealed similar trends, with smaller differences to the Pd(111) surface energies. The only deviation with respect to the Ag/Pt(111) systems is again the Ag1L system, where for Ag/Pd(111) the difference with respect to Pd(111) is marginal and even negative, while for Ag/Pt(111) this was positive and biggest. The generally more Ag(111)-like surface energies of the Ag/Pd(111) systems indicate that the electronic properties of the Ag surface layer are less affected by the underlying Pd layers than this is the case for the Ag/Pt(111) systems. In particular, the long-range effects observed for the Ag1L system in the Ag/Pt(111) case are absent.

3.2.3. Surface Energies from Cleaving the 12 Layer Slabs. Finally, we also calculated surface energies of the Ag-terminated surfaces of the different Ag/Pt(111) and Ag/Pd(111) systems by cleaving the symmetric, Pt-terminated 12-layer slabs, which results in the asymmetric 6-layer slabs shown in Figure 2. The resulting surface energies, which are listed in Table S2, closely resemble the values obtained for the Ag-terminated 12-layer slab via eq 3 (Table S1). The small differences of at most ±1 meV Å^{-2} are mainly due to the additional relaxation of the Ag layers upon cleaving, i.e., slight differences in the structure of the Ag layers compared to the Ag-terminated 12-layer system.

In total, the data presented in Section 3.2 clearly demonstrate the difference between the average surface energies calculated via eq (2), which can easily be calculated from Table S1, and the surface energies calculated via eqs 3 and 4. For the comparable Ag/Pd(111) systems the trends are generally similar, but with distinct differences in the surface energies of the Ag1L system. Finally, the data also illustrate the magnitude of possible discrepancies when determining the surface energy of the deposit side of an asymmetric bimetallic Ag/Pt(111) slab via assuming the surface energy of Pt(111) for the bottom side.

3.3. Formation Energies of Different Bimetallic Ag/Pt(111) Systems. *3.3.1. Bulk Formation Energies of Ag-Terminated PtAg Systems.* For the calculation of the formation energies E_f of these bimetallic systems, we can use the approach described in eq 9. Normalizing to the number of surface metal atoms n_s we obtain for the bulk formation energy $E_{f,bulk}$

$$E_{f,bulk} = \frac{1}{n_s}\left(E_{bulk} - \sum_i n_i \cdot E_{b,i}\right) \tag{13}$$

where i denotes the different metal atoms in the bulk unit cell (Pt, Ag). The resulting bulk formation energies are plotted as orange bars in Figure 5a and listed in Table S1.

Most important finding is that all formation energies $E_{f,bulk}$ are positive, i.e., the formation of the bimetallic bulk units cells with atoms from the respective reservoirs costs energy. Hence, for these specific systems phase separation into Ag and Pt would be more favorable.

3.3.2. Compression and Interface Energies of Ag-Terminated PtAg Systems. As described in Section 3.1, the bulk formation energies contain contributions from the compression of the guest material in the pseudomorphic films, in this case Ag, and from additional interactions between Ag and Pt, on top of the average of the Ag−Ag and Pt−Pt interactions. In a simple picture, e.g., for the description of a deposit Ag film on a metallic Pt(111) substrate, this is also termed as interface energy.

The compression energies of the different Ag/Pt(111) systems, which are indicated as gray bars in Figure 5a, were calculated via the Ag compression energy per Ag atom, $E^0_{Ag_{Pt}}$, using the 12-layer Ag unit cell once with the natural lattice and once with the vertically relaxed Pt(111) lattice (see eq 8). As expected, the compression energies are positive and increase steadily from the Ag1L to the Ag3L system. For the mixed layer in the Pt_1Ag_3 systems, where the Ag compression and

https://doi.org/10.1021/acs.jpcc.4c02619
J. Phys. Chem. C 2024, 128, 13558−13567

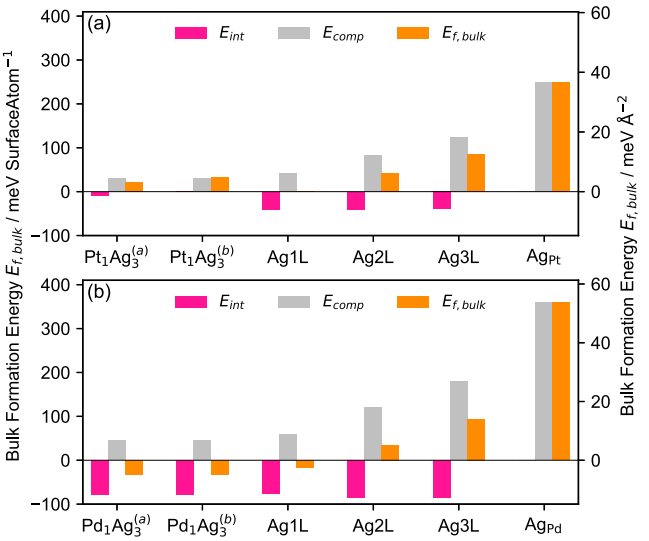

Figure 5. (a) Bulk formation energies $E_{f,bulk}$, compression energies E_{comp} and interface energies E_{int} of the Ag-terminated symmetric Ag/Pt(111) 12-layer unit cells of different bimetallic Ag/Pt(111) systems and of the compressed Ag bulk. (b) Similar data for Ag/Pd(111) systems. For comparison with surface energies, we also provided an energy scale in meV Å^{-2} at the right axis. The energies given in the figure are characteristic for a 6-layer slab with 24 atoms, exact values are listed in Table S1.

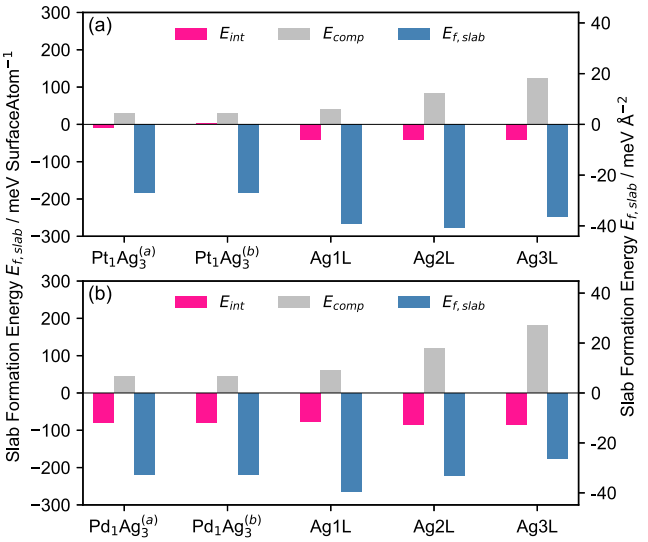

Figure 6. (a) Slab formation energies $E_{f,slab}$ (blue bars), compression energies E_{comp} (gray bars) and interface energies E_{int} (red bars) of the Ag-terminated symmetric Ag/Pt(111) 12-layer slabs of different bimetallic Ag/Pt(111) systems (for details, see text). (b) Similar data for the Ag/Pd(111) systems. The energies given in the figure are characteristic for a 6-layer slab with 24 atoms, the exact values are listed in Table S1.

thus the compression energy are not well-defined, we estimated the compression energy as 3/4 of the compression energy in the Ag1L system, based on the $Pt_{0.25}Ag_{0.75}$ composition. Therefore, this should be considered as a qualitative estimate.

The (compression corrected) interface energies, calculated via eqs 6 and 7, are plotted as red bars in Figure 5a. For the Ag_{Pt} system this is zero by definition. For the Ag film covered systems, we obtain slightly negative values. Hence, the interaction between the Pt and the laterally compressed, pseudomorphic Ag films is weakly attractive, slightly stronger than the mean Pt−Pt and Ag−Ag interactions. The positive character of the bulk formation energies is therefore dominated by the positive contribution from the Ag compression.

3.3.3. Slab Formation Energies of the Ag-Terminated PtAg Systems. For comparison, we also calculated the slab formation energies for the different Ag/Pt(111) systems via eq 10. The resulting values are plotted as blue bars in Figure 6a and listed in Table S1. For better visualization, we also included the compression energies (gray bars) and interface energies (red bars), which by definition are identical to those in the bulk unit cell (Figure 5a).

Considering that eq 10 can also be rewritten as

$$E_{f,slab} = \frac{1}{2A}\left(E_{slab} - \sum_i n_i \cdot E_{b,i} - E_{S_{Pt(111)}}\right) \quad (14)$$

it is the high surface energy of Pt(111) which is responsible for the negative character of the slab formation energies. In other words, the pronounced change in surface energy, which is present in the slab formation energy, but not in the bulk formation energy, is responsible for the pronounced difference between (positive) bulk formation energies and (negative) slab formation energies in the Ag/Pt(111) systems.

Also here we calculated the respective energies for the Ag/Pd(111) systems. The resulting values are presented in Figures 5b and 6b and in Table S1. Generally, the trends are rather similar, but with differences in the absolute values and in specific systems. The bulk formation energies are mostly slightly lower than for the corresponding Ag/Pt(111) systems, and some are even negative. Again, the bulk formation energies increase with increasing Ag film thickness, and the increase is more pronounced than for the Ag/Pt(111) systems. This is mostly due to the larger contribution of the compression energies, which are caused by the slightly smaller lattice constant of Pd(111) compared to Pt(111). Although the difference is small, the effect on the compression energy is significant. On the other hand, the bulk formation energy of the Ag1L system is even negative for Ag/Pd(111), while it is positive for Ag/Pt(111). This is due to the much larger (negative) interface energy in the Ag/Pd(111) system. In fact, the interface energies are generally larger (and negative) in the Ag/Pd(111) systems than in the Ag/Pt(111) systems, by about a factor of 2, reflecting the tendency for intermixing due to a relatively stronger Pd−Ag bonding. This further supports our above conclusion of stronger interactions between Ag and Pd than between Ag and Pt, relative to the Pd−Pd (Pt−Pt) interactions and Ag−Ag interactions. Based on these trends, we would expect a higher tendency for intermixing (alloy formation) in the Ag/Pd(111) system than for the Ag/Pt(111) system, which is fully consistent with experimental observations. Finally, different from Ag/Pt(111), the bulk formation energies of the Pd/Ag1L surface alloys are not higher than those of the Ag1L film system, but lower. This results from the lower compression energy in the surface alloys than in Ag1L, in combination with similar size interface energies.

Similar trends are also observed in the slab formation energies of the Ag/Pd(111) systems, which include also changes in the surface energies (see Figure 6b and Table S1).

Finally, we would also like to comment on the tendency for two-dimensional phase separation in the surface layer of the surface, which was indicated by scanning tunneling microscopy

https://doi.org/10.1021/acs.jpcc.4c02619
J. Phys. Chem. C 2024, 128, 13558−13567

data for PtAg/Pt(111) monolayer surface alloys.[13,16,18] Comparing the slab formation energies of −39.35 meV A^{-2} for the Ag1L system and −26.82 meV A^{-2} for the Pt_1Ag_3/Pt(111) surface alloys (see Table S1), we get mean formation energies of 3/4 × −39.35 = −29.5 meV A^{-2} for the phase separated Pt_1Ag_3/Pt(111) system which is favorable compared to the formation energy of −26.82 meV A^{-2} of the mixed surface layer (Pt_1Ag_3), in good qualitative agreement with the experimental observation. In contrast, for Pd_1Ag_3/Pd(111) surface alloys, which show a random distribution of the Pd and Ag surface atoms,[8] a similar calculation results in (mean) formation energies of 3/4 × −39.57 = −29.7 meV A^{-2} for the phase separated surface and −32.50 meV A^{-2} for the mixed phase, which favors 2D intermixing, in good agreement with experimental observations.[8]

3.3.4. Comparison between Formation Energies between Mirrored and Stacked 6-Layer Bulk Cells. To complete the picture, we checked for possible differences in the formation energies calculated via the symmetric 12-layer bulk unit cell (Figure 1) and that obtained for a stacked, asymmetric 6-layer bulk unit cell for the different Ag/Pt(111) systems (Figure 7a).

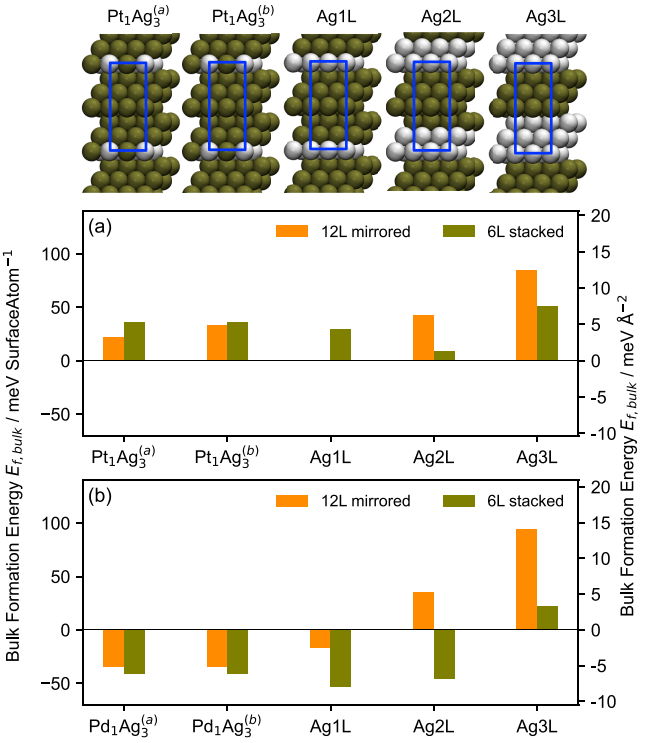

Figure 7. Schematic representation of the stacked (nonmirrored), asymmetric unit cell and bulk formation energies E_f of the different Ag/Pt(111) (a) and Ag/Pd(111) (b) systems for the symmetric 12-layer unit cell (see Figure 2) and the stacked, asymmetric 6-layer unit cell. Note the different number of Pt−Ag interfaces as compared to the structures in Figure 2 (see also text). The energies given in the figure are characteristic for a 6-layer slab with 24 atoms. The exact values are listed in Table S3.

This 6-layer cell differs from that in Figure 2 in that in the previous case two asymmetric 6-layer unit cells were mirrored to form the symmetric 12-layer unit cell, while in the present they are sequentially stacked. The main difference between these systems is in the number of (pseudomorphic) Pt−Ag interfaces. In the mirrored 12-layer system there are 2 interfaces between Ag layer(s) and (vertically) relaxed Pt layers per 12-layer system, while in the stacked, asymmetric system there are 2 interfaces between Ag layers and unrelaxed Pt layers and 2 more interfaces between Ag and relaxed Pt layers per 12-layer system. The formation energies of the bimetallic unit cells were again calculated via eq 10. The resulting formation energies of the two different types of unit cells, which again include contributions from interface energies and compression energies, are plotted in Figure 7 and listed in Table S3.

Obviously, there are clearly detectable differences between the formation energies of the stacked and the mirrored systems, which must be due to the different types and numbers of interfaces in the two cell types. These include 2 Ag−Pt_{rel} interfaces (Pt_{rel}: relaxed Pt) in the symmetric, mirrored 12-layer unit cell and 4 Ag−Pt_{fix} interfaces (Pt_{fix}: fixed Pt) in 2 unit cells with together 12 layers for the stacked, asymmetric unit cells. Also, the Ag−Ag bonds between Ag layers are replaced by Ag−Pt_{fix} bonds. The compression energies, in contrast, should be identical in both cases, since in these calculations all Ag layers are pseudomorphic. Important to note is that the compression energies were mainly responsible for the increasing bulk formation energy from the Ag1L via the Ag2L to the Ag3L system. In summary, for the Ag-film systems the differences between symmetric 12-layer and stacked asymmetric 6-layer system are quite significant, relative to the absolute formation energies. Interestingly, for the Ag1L system the 6-layer stacked system is energetically more costly than the 12-layer system, indicating that the formation of the 4 Ag: Pt_{fix} interfaces costs more energy than the 2 Ag−Pt_{rel} interfaces. For the Ag2L systems, it is just opposite. In that case the formation of the 4 Ag/Pt_{fix} interfaces is favorable. Finally, for the Ag3L system the situation is comparable to that in the Ag1L system. Hence, even details of the interface structure can have a sizable effect on the bulk formation energies. As a result, the artificial assumption of two bulk-like Pt bottom layers in the bulk unit cell, which interact with relaxed layers on both sides, can have detectable consequences on the bulk formation energies, which will appear also in the slab formation energies and in the surface energies.

For the corresponding Ag/Pd(111) systems the general trends are comparable. However, as discussed before with Figure 4, the formation energies are more negative than for Ag/Pt(111), and the Ag compression energy is larger, due to the slightly smaller lattice constant of Pd compared to Pt. Main difference between the Ag12L and the Ag6L systems is that for Ag/Pt(111) the bulk formation energies are always more negative than for the Ag12 L systems. Hence, in this case the formation of the four Ag−Pd_{fix} interfaces is always more favorable than the formation of two Ag−Pt_{rel} interfaces. This is in full agreement with our previous conclusion of more facile intermixing for the Pd−Ag system than for Pt−Ag, due to the stronger bonding between Pd and Ag.

In total, the data presented in Section 3.3 clearly illustrate the difference between bulk formation and slab formation energies. The significant contributions of interface and compression energies could be quantified. The tendency for surface intermixing or 2D phase separation in the topmost bimetallic layer on Pt(111) or Pd(111) could be derived from the slab formation energies. Finally, the data demonstrate that even the relaxation of the Pt (Pd) bottom layers of the symmetric slabs can have a small, but detectable effect on the formation energies and thus on the surface and interface energies of the Ag/Pt(111) and Ag/Pd(111) systems. This

https://doi.org/10.1021/acs.jpcc.4c02619
J. Phys. Chem. C 2024, 128, 13558−13567

underlines the importance of the correct choice of the respective reference system and its structure, as well as their clear definition.

3.4. Comparison with Experimental Data. Comparison of the calculated data presented in the previous sections with experimental data is cumbersome because of two reasons. First, a large fraction of the systems explored here are either experimentally not accessible, or, if they do exist, not stable under experimental conditions. Second, there are no simple and straightforward experiments giving access to surface energies, interface energies, etc.

For the present systems, a closely related experimental study was reported by Paffett et al.[38] They showed by temperature-programmed desorption that the Ag atoms in a pseudomorphic monolayer on Pt(111) bind 3.8 ± 2 kcal/mol more strongly to Pt(111) than the Ag atoms bind to the surface of bulk Ag(111). Here one has to keep in mind that upon heating the Ag/Pt(111) surface to high temperatures (desorption temperature), also exchange and intermixing processes are activated, as known from scanning tunneling microscopy (STM) experiments.[14,18] Hence, desorption partly occurs from a PtAg/Pt(111) surface alloy. In that case, lateral ligand effects are likely to play a role as well, which have to be considered in the evaluation of the desorption kinetics and in the binding energy derived from these measurements. Hence, such kind of experiment can be interpreted in a straightforward way only for systems where exchange and intermixing processes are kinetically inhibited even at desorption temperatures, as known, e.g., for Ag desorption from Ru(0001).[39]

Furthermore, the direct comparison of this difference in Ag adsorption energies on the two substrates with the calculated data is, however, not possible. For the case of a pseudomorphic monolayer Ag deposit on a Pt(111) substrate or on a Ag(111) substrate, respectively, the measured difference in binding energies includes contributions from the difference in surface energies for Ag/Pt(111) and Ag/Ag(111), the difference in compression energies, and the additional presence of the interface energy in Ag/Pt(111). Using the numbers given in Tables S1−S3, the interface energy and the compression energy essentially cancel each other out for the Ag/Pt(111) system, while for Ag/Ag(111) these contributions are zero per se. Assuming then that the interface energies are identical in the bulk system and in the slab, only the difference in the surface energies remains, which is about 9.58 meV Å^{-2} (see Table S1). Considering that there are 4 surface atoms per (2 × 2) unit cell with 30.8 Å^2 (1 kcal mol^{-1} = 0.0434 eV particle^{-1}), we obtain a difference of about 1.7 kcal mol^{-1} as compared to the experimental value of 3.8 ±2 kcal mol^{-1}. Considering the approximations in this estimate and the uncertainties in absolute values of the calculated surface energies, we find this agreement very close.

4. CONCLUSIONS

We have derived concepts for determining thermodynamic surface properties such as surface energies, formation energies, interface energies, or compression energies of bimetallic surfaces from first-principles, employing periodic density functional theory calculations and using larger, symmetric unit cells and slabs. This way we could determine the properties of the asymmetric surface region without interference with contributions from the bottom side of the slabs used in these calculations.

These concepts were employed to determine the above surface properties of bimetallic Ag/Pt(111) and, for comparison, of Ag/Pd(111) surfaces, including pseudomorphic Ag film covered surfaces and M_xAg_{1-x}/M(111) (M = Pt, Pd) monolayer surface alloys.

In general, we obtained similar trends for Ag/Pt(111) surfaces and Ag/Pd(111) surfaces, but with differences in the absolute values and specific exceptions. Surface energies of the Ag film covered surfaces were generally close to that of the Ag(111) surface, with the exception of the monolayer Ag covered Pt(111) surface, while for the similar Ag/Pd(111) surface it was Ag(111) like. This discrepancy points to specific interactions between the Ag monolayer and Pt(111), which are absent in the other cases. Formation energies were shown to differ significantly when using bulk or slab systems, which mainly reflects the fact that the latter ones include also changes in the surface energy, which can dominate the formation energy. As a result, bulk based formation energies are always positive for Ag/Pt(111) systems, but partly negative for Ag/Pd(111) systems, while slab based formation energies are always negative. Interface energies, reflecting the additional interaction between Ag and the host metal M as compared to the average of the Ag−Ag and M−M interactions, are derived from appropriately structured bulk unit cells, and corrected for contributions arising from the compression of the film layers (compression energy). They were found to be higher for the Ag/Pd(111) than for the Ag/Pt(111) systems, pointing to a stronger driving force for intermixing in the former case, while the latter system tends to phase separation.

In a general sense, the study provided a tool box for the determination of thermodynamic surface properties of asymmetric heterogeneous surface regions, specifically of bimetallic surfaces, from DFT calculations. Furthermore, it demonstrates the importance of the proper choice and of the clear indication of the reference system, as illustrated, e.g., for the difference between formation energies in bulk or slab systems.

■ ASSOCIATED CONTENT

Data Availability Statement

The optimized atomic coordinates of the DFT calculations and a summary spreadsheet are available in Zenodo at 10.5281/zenodo.12564927.

Supporting Information

The Supporting Information is available free of charge at https://pubs.acs.org/doi/10.1021/acs.jpcc.4c02619.

> Derivation of eq 11 as well as tables with the surface energies, interface energies, compression energies and formation energies for symmetric 12L bimetallic (111) oriented structures (48 atoms), with the surface energies of the asymmetric, mirrored 6-layer bimetallic (111) oriented structures (24 atoms) and with the formation energies of the asymmetric, stacked 6L bimetallic (111) oriented structures (Figure 7) (PDF)

■ AUTHOR INFORMATION

Corresponding Author

R. Jürgen Behm − *Institute of Theoretical Chemistry, Ulm University, D-89081 Ulm, Germany;* orcid.org/0000-0002-7565-0628; Email: juergen.behm@uni-ulm.de

https://doi.org/10.1021/acs.jpcc.4c02619
J. Phys. Chem. C 2024, 128, 13558−13567

Authors

Sung Sakong − *Institute of Theoretical Chemistry, Ulm University, D-89081 Ulm, Germany;* orcid.org/0000-0001-9777-7489

Axel Groß − *Institute of Theoretical Chemistry, Ulm University, D-89081 Ulm, Germany;* orcid.org/0000-0003-4037-7331

Complete contact information is available at: https://pubs.acs.org/10.1021/acs.jpcc.4c02619

Notes

The authors declare no competing financial interest.

■ ACKNOWLEDGMENTS

Computational resources were provided by the federal state of Baden Württemberg through the bwHPC initiative and by the German Science Foundation (DFG) under grant no INST40/575-1 FUGG (JUSTUS 2 cluster).

■ REFERENCES

(1) Bauer, E. Phänomenologische Theorie der Kristallabscheidung an Oberflächen I. *Z. Kristallogr.* **1958**, *110*, 372−394.

(2) Bauer, E. Phänomenologische Theorie der Kristallabscheidung an Oberflächen II. *Z. Kristallogr.* **1958**, *110*, 395−431.

(3) Groß, A. *Theoretical Surface Science: A Microscopic Perspective*, 1st ed.; Springer, 2007; pp 1−90.

(4) Groß, A. Adsorption at Nanostructured Surfaces from First Principles. *J. Comput. Theor. Nanosci.* **2008**, *5*, 894−922.

(5) Yu, W.; Porosoff, M. D.; Chen, J. G. Review of Pt-Based Bimetallic Catalysis: From Model Surfaces to Supported Catalysts. *Chem. Rev.* **2012**, *112*, 5780−5817.

(6) Ma, Y.; Bansmann, J.; Diemant, T.; Behm, R. J. Formation, Stability and CO Adsorption Properties of PdAg/Pd(111) Surface Alloys. *Surf. Sci.* **2009**, *603*, 1046−1054.

(7) Ma, Y.; Diemant, T.; Bansmann, J.; Behm, R. J. The Interaction of CO with PdAg/Pd(111) Surface Alloys - A Case Study of Ensemble Effects on a Bimetallic Surface. *Phys. Chem. Chem. Phys.* **2011**, *13*, 10741−10754.

(8) Engstfeld, A. K.; Hoster, H. E.; Behm, R. J. Formation, Atomic Distribution and Mixing Energy in Two-Dimensional Ag_xPd_{1-x} Surface Alloys on Pd(111). *Phys. Chem. Chem. Phys.* **2012**, *14*, 10754−10761.

(9) Farkas, A. P.; Diemant, T.; Bansmann, J.; Behm, R. J. The Adsorption of Oxygen and Coadsorption of CO and Oxygen on PdAg/Pd(111) Surface Alloys. *ChemPhysChem* **2012**, *13*, 3516−3525.

(10) Mancera, L. A.; Behm, R. J.; Groß, A. Structure and Local Reactivity of PdAg/Pd(111) Surface Alloys. *Phys. Chem. Chem. Phys.* **2013**, *15*, 1497−1508.

(11) Mancera, L. A.; Diemant, T.; Groß, A.; Behm, R. J. Molecular and Dissociative Hydrogen Adsorption on Bimetallic PdAg/Pd(111) Surface Alloys: A Combined Experimental and Theoretical Study. *J. Phys. Chem. C* **2022**, *126*, 3060−3077.

(12) Diemant, T.; Schüttler, K. M.; Behm, R. J. Ag on Pt(111): Changes in Electronic and CO Adsorption Properties upon PtAg/Pt(111) Monolayer Surface Alloy Formation. *ChemPhysChem* **2015**, *16*, 2943−2952.

(13) Schüttler, K.; Mancera, L. A.; Diemant, T.; Groß, A.; Behm, R. J. Interaction of CO With Pt_xAg_{1-x}/Pt(111) Surface Alloys: More than Dilution by Ag Atoms. *Surf. Sci.* **2016**, *650*, 237−254.

(14) Beckord, S.; Engstfeld, A. K.; Brimaud, S.; Behm, R. J. Electrochemical Characterization and Stability of Ag_xPt_{1-x}/Pt(111) Surface Alloys. *J. Phys. Chem. C* **2016**, *120*, 16179−16190.

(15) Beckord, S.; Brimaud, S.; Behm, R. J. Stability and ORR Performance of a Well-Defined Bimetallic $Ag_{70}Pt_{30}$/Pt(111) Monolayer Surface Alloy Electrode - Probing the De-Alloying at an Atomic Scale. *Electrochim. Acta* **2018**, *259*, 762−771.

(16) Beckord, S.; Brimaud, S.; Behm, R. J. The Performance of Structurally Well-Defined Ag_xPt_{1-x}/Pt(111) Surface Alloys in the Oxygen Reduction Reaction - An Atomic-Scale Picture. *J. Electroanal. Chem.* **2018**, *819*, 401−409.

(17) Andersen, O. K. Electronic Structure of the Fcc Transition Metals Ir, Rh, Pt, and Pd. *Phys. Rev. B* **1970**, *2*, 883−906.

(18) Rötter, R. *Atomverteilung in Zweidimensionalen Pt_xAg_{1-x} Legierungen auf Pt(111)*; Ulm University, 2009.

(19) Mancera, L. A.; Groß, A.; Behm, R. J. Stability, Electronic Properties and CO Adsorption Properties of Bimetallic PtAg/Pt(111) Surfaces. *Phys. Chem. Chem. Phys.* **2024**, *26*, 18435−18448, DOI: 10.1039/D4CP01640H.

(20) Nikitin, I.; Dong, W.; Busnengo, H. F.; Salin, A. Diffusion of a Hydrogen Atom on the Pd(1 1 1) Surface: Quantum Transition State Wave Packet Approach. *Surf. Sci.* **2003**, *547*, 149−156.

(21) Hong, S.; Rahman, T. S. Adsorption and Diffusion of Hydrogen on Pd(211) and Pd(111): Results From First-Principles Electronic Structure Calculations. *Phys. Rev. B* **2007**, *75*, No. 155405.

(22) Fearon, J.; Watson, G. W. Hydrogen Adsorption and Diffusion on Pt {111} and PtSn {111}. *J. Mater. Chem.* **2006**, *16*, 1989−1996.

(23) Seebauer, E. G.; Schmidt, L. D. Surface Diffusion of Hydrogen on Pt(111): Laser-Induced Thermal Desorption Studies. *Chem. Phys. Lett.* **1986**, *123*, 129−133.

(24) Kwasniewski, V. J.; Schmidt, L. D. Surface Diffusion of CO on Pt(111). *Surf. Sci.* **1992**, *274*, 329−340.

(25) Šnábl, M.; Borusík, O.; Cháb, V.; Ondrejcek, M.; Stenzel, W.; Conrad, H.; Bradshaw, A. M. Surface Diffusion of CO Molecules on Pd{111} Studied With Photoelectron Emission Microscopy. *Surf. Sci.* **1997**, *385*, L1016−L1022.

(26) Mitsui, T.; Rose, M.; Fomin, E.; Ogletree, D.; Salmeron, M. Diffusion and Pair Interactions of CO Molecules on Pd(111). *Phys. Rev. Lett.* **2005**, *94*, No. 036101.

(27) Kresse, G.; Furthmüller, J. Efficient Iterative Schemes for Ab Initio Total-Energy Calculations Using a Plane-Wave Basis Set. *Phys. Rev. B* **1996**, *54*, 11169−11186.

(28) Perdew, J. P.; Burke, K.; Ernzerhof, M. Generalized Gradient Approximation Made Simple. *Phys. Rev. Lett.* **1996**, *77*, 3865−3868.

(29) Blöchl, P. E. Projector Augmented-Wave Method. *Phys. Rev. B* **1994**, *50*, 17953−17979.

(30) Kresse, G.; Joubert, D. From Ultrasoft Pseudopotentials to the Projector Augmented-Wave Method. *Phys. Rev. B* **1999**, *59*, 1758−1775.

(31) Kresse, G.; Furthmüller, J. Efficiency of Ab-Initio Total Energy Calculations for Metals and Semiconductors Using a Plane-Wave Basis Set. *Comput. Mater. Sci.* **1996**, *6*, 15−50.

(32) Wyckoff, R. A. L. P. *Crystal Structures*; Interscience Publ.: New York, 1963.

(33) Barabash, S. V.; Blum, V.; Müller, S.; Zunger, A. Prediction of Unusual Stable Ordered Structures of Au-Pd Alloys Via First-Principles Cluster Expansion. *Phys. Rev. B* **2006**, *74*, No. 035108.

(34) Tersoff, J. Surface-Confined Alloy Formation in Immiscible Systems. *Phys. Rev. Lett.* **1995**, *74*, 434−437.

(35) Brune, H.; Röder, H.; Boragno, C.; Kern, K. Strain Relief at Hexagonal-Close-Packed Interfaces. *Phys. Rev. B* **1994**, *49*, 2997−3000.

(36) Rangelov, G.; Fauster, T.; Strüber, U.; Küppers, J. Stacking of Ag Layers on Pt(111). *Surf. Sci.* **1995**, *331−333*, 948−951.

(37) Gohda, Y.; Groß, A. Structure-Reactivity Relationships for Bimetallic Electrodes: Pt Overlayers and PtAu Surface Alloys on Au(111). *J. Electroanal. Chem.* **2007**, *607*, 47−53.

(38) Paffet, M. T.; Campbell, C. T.; Taylor, T. N. Surface Chemical Properties of Ag/Pt(111): Comparisons Between Electrochemistry and Surface Science. *Langmuir* **1985**, *1*, 741−747.

(39) Niemantsverdriet, J. W.; Dolle, P.; Markert, K.; Wandelt, K. Thermal Desorption of Strained Monoatomic Ag and Au Layers From Ru(001). *J. Vac. Sci. Technol., A* **1987**, *5*, 875−878.